Using Eu3+ as an atomic probe to investigate the local environment in LaPO4–GdPO4 monazite end-members

Huittinen, N.; Arinicheva, Y.; Schmidt, M.; Neumeier, S.; Stumpf, T.;

Originally published:

August 2016

Journal of Colloid and Interface Science 483(2016), 139-145

DOI: https://doi.org/10.1016/j.jcis.2016.08.027

Perma-Link to Publication Repository of HZDR:

https://www.hzdr.de/publications/Publ-24093

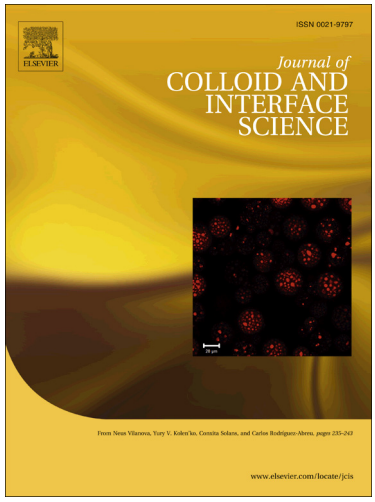

Using Eu^{3+} as an atomic probe to investigate the local environment in $LaPO_4$–$GdPO_4$ monazite end-members

Nina Huittinen, Yulia Arinicheva, Moritz Schmidt, Stefan Neumeier, Thorsten Stumpf

PII: S0021-9797(16)30582-3
DOI: http://dx.doi.org/10.1016/j.jcis.2016.08.027
Reference: YJCIS 21495

To appear in: *Journal of Colloid and Interface Science*

Received Date: 27 May 2016
Revised Date: 5 August 2016
Accepted Date: 10 August 2016

Please cite this article as: N. Huittinen, Y. Arinicheva, M. Schmidt, S. Neumeier, T. Stumpf, Using Eu^{3+} as an atomic probe to investigate the local environment in $LaPO_4$–$GdPO_4$ monazite end-members, *Journal of Colloid and Interface Science* (2016), doi: http://dx.doi.org/10.1016/j.jcis.2016.08.027

Using Eu^{3+} as an atomic probe to investigate the local environment in $LaPO_4$-$GdPO_4$ monazite end-members

Nina Huittinen[1*], Yulia Arinicheva[2], Moritz Schmidt[1], Stefan Neumeier[2], Thorsten Stumpf[1]

[1]Helmholtz-Zentrum Dresden - Rossendorf, Institute of Resource Ecology, Bautzner Landstraße 400, 01328 Dresden, Germany

[2]Forschungszentrum Jülich GmbH, Institute of Energy and Climate Research, Nuclear Waste Management and Reactor Safety (IEK-6), 52425 Jülich, Germany

E-mail addresses of all authors in order of appearance : n.huittinen@hzdr.de, y.arinicheva@fz-juelich.de, moritz.schmidt@hzdr.de, s.neumeier@fz-juelich.de, t.stumpf@hzdr.de

*Corresponding author :

Nina Huittinen / n.huittinen@hzdr.de

Phone : +49 351 260 2148

Fax : +49 351 260 13233

Abbreviations used in the article:

Time-resolved laser fluorescence spectroscopy (TRLFS)

Abstract

In the present study, we have investigated the luminescent properties of Eu^{3+} as a dopant in a series of synthetic lanthanide phosphates from the monazite group. Systematic trends in the spectroscopic properties of Eu^{3+} depending on the size of the host cation and the dopant to ligand distance have been observed. Our results show that the increasing match between host and dopant radii when going from Eu^{3+}-doped $LaPO_4$ toward the smaller $GdPO_4$ monazite decreases both the full width at half maximum of the Eu^{3+} excitation peak, as well as the $^7F_2/^7F_1$ emission band intensity ratio. The decreasing Ln···O bond distance within the $LnPO_4$ series causes a systematic bathochromic shift of the Eu^{3+} excitation peak, showing a linear dependence of both the host cation size and the Ln···O distance. The linear relationship can be used to predict the energy band gap for Eu^{3+}-doped monazites for which no Eu^{3+} luminescent data is available. Finally, mechanisms for metal-metal energy transfer between host and dopant lanthanides have been explored based on recorded luminescence lifetime data. Luminescence lifetime data for Eu^{3+} incorporated in the various monazite hosts clearly indicated that the energy band gap between the guest ion emission transition and the host ion absorption transition can be correlated to the degree of quenching observed in these materials with otherwise identical geometries and chemistries.

keywords : Eu^{3+}, monazite, incorporation, TRLFS, luminescence, quenching

1 Introduction

Crystalline lanthanide orthophosphates ($LnPO_4$) doped with other elements of the lanthanide group have recently gathered substantial attention due to the favorable electronic properties of the 4*f* elements that can be employed for applications ranging from light display systems[1] and nanoelectronic devices[2], medical and biological labels for in vitro imaging[3] to applications in targeted drug release[4]. Orthophosphates offer an easily synthesized and robust solid matrix for the dopants, and $LnPO_4$ nanoparticles can be tailored for a variety of purposes. The chemical durability and structural flexibility of $LnPO_4$ make lanthanide phosphates crystallizing in the monazite structure attractive as host phases for the conditioning of long-lived radionuclides produced during the nuclear fuel cycle or in the dismantling of nuclear weapons.[5-10] The monazites are known to incorporate large quantities of actinides (> 20%)[6,11], and several studies report on the structural incorporation of actinides such as U, Th, Pu, Am, and Cm, within the monazite structure either through direct substitution by a trivalent actinide on the host cation site[12,13], or through coupled substitution of an actinide of higher oxidation state with a mono- or divalent cation to preserve charge neutrality[14,15]. Eu^{3+} is often chosen as dopant in the investigated phosphates mainly due to its luminescent properties. Eu^{3+} is a preferred choice as an activator ion in the development of red-emitting phosphors due to its strong, long-lived luminescence emission.[16,17] Furthermore, crystal-field perturbation results in a fine structure in the luminescence spectra that depends on the site symmetry of the Eu^{3+} ion which, thus, can be used as a local structure probe for the determination of site symmetries in a host lattice.[18] In general, luminescent properties of lanthanide ions depend on the host composition and structure as well as the concentration (i.e. interatomic distance) of luminescent centers present in the materials.[19-22] Therefore, local changes in the host material and the concentration range of dopants used will alter the spectroscopic properties of the luminescent probe and, depending on the application, may affect the suitability of the material.

In the present work we have studied Eu^{3+} incorporation and the impact of systematic trends within the host crystal structure on the dopant luminescence in a series of $LnPO_4$ end-members ($LaPO_4$-$GdPO_4$) crystallizing in the monazite structure. The ionic radius of the host cation in these monazite end-members decreases systematically from La^{3+} (r_{ion}^{IX} = 1.216 Å)[23] toward Gd^{3+} (r_{ion}^{IX} = 1.107 Å)[21] by ~10 %. A preferential incorporation of Eu^{3+} in monazites with a host cation radius similar to Eu's (r_{ion}^{IX} = 1.120 Å)[23], e.g. $SmPO_4$ or $GdPO_4$, could be expected. In addition, the systematic decrease of the Ln···O bond distance in the series of monazite hosts with otherwise identical symmetry and chemistry provides an opportunity to study the impact of bond distance on the ligand field effect and the luminescent properties of the Eu^{3+} ion. Finally, by comparing the Eu^{3+} doped monazites with isolated fluorescent centers (c_{Eu} = 500 ppm) with pure $EuPO_4$, the influence of the lanthanide concentration in terms of metal-metal concentration quenching effects can be evaluated.

2 Experimental section

2.1 Lanthanide phosphate synthesis and characterization

The lanthanide phosphates $LaPO_4$ to $GdPO_4$ crystallizing in the monazite structure were synthesized by precipitation (excluding the redox sensitive $CePO_4$ and radioactive $PmPO_4$) similar to the procedure described in Roncal-Herrero et al.[24]

Lanthanide nitrate salts were dissolved in deionized water (MilliQ) in concentrations of 0.3-0.5 M. A 14.8 M aqueous solution of H_3PO_4 was slowly added to the solution, causing precipitation of $LnPO_4$:Eu^{3+} according to Reaction 1. Details on the reagents used in the synthesis can be found in the supporting information (S.I.).

$$Ln(NO_3)_3 + H_3PO_4 \xrightarrow{500\ ppm\ Eu^{3+}} LnPO_4{:}Eu^{3+} + 3HNO_3 \qquad \text{(Reaction 1)}$$

The suspension was heated in an oven at 90°C for 1 week to complete the precipitation. The solid was recovered by centrifugation (10,000 rpm, 10 min) and washed with MilliQ water. The washing step was repeated several times until the supernatant was free of nitrate ions (NO_3^- test strips). Subsequently the powders were dried in an oven at 90 °C for 12 h. The dry powders were milled in an agate mortar and calcined for 2h at 600°C in order to remove any nitrate residues. As a final step, sintering of $LnPO_4$ was carried out at 1450°C for 5h to obtain the crystalline monazite solids. Characterization of the synthetic monazites was done with X-ray powder diffraction (XRD), using a D4 Endeavor diffractometer with a θ–2θ geometry (Bruker AXS GmbH) operating at 50 kV and 30 mA with a CuKα radiation (λ = 1.5418 Å) in the range 2θ = 10–100°. The XRD patterns of all synthesized monazites are in a perfect agreement with the corresponding data from the ICDD database, confirming the sole presence of highly crystalline, monoclinic monazite. XRD patterns for pure $EuPO_4$ and Eu^{3+}-doped $GdPO_4$ are shown in Figure 1. For the XRD patterns of all synthetic monazites the reader is referred to the S.I., Figure S1.

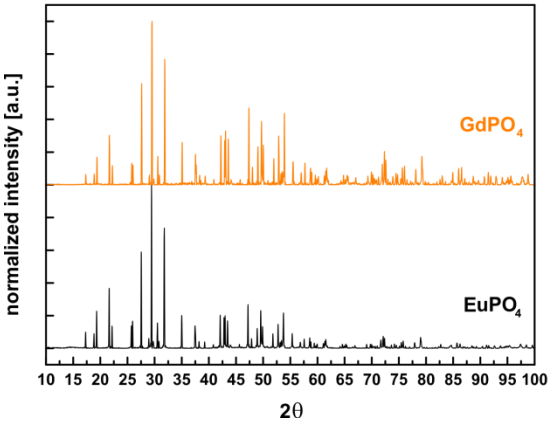

Figure 1: XRD patterns of synthetic $EuPO_4$ monazite and Eu^{3+}-doped $GdPO_4$ monazite.

2.2 Time-resolved laser fluorescence spectroscopy TRLFS

The Eu^{3+} ion exhibits many favorable luminescence properties, such as a non-degenerate ground state ($^7F_0$) as well as emitting state ($^5D_0$) and an even number of *f*-electrons ($4f^6$) for which the number of crystal field levels is dependent on the site symmetry of the ion.[25] Therefore, Eu^{3+} is ideally suited for systematic studies of the structural incorporation of Eu^{3+} in crystalline solid phases, such as this series of synthetic monazites.

Detailed information on the Eu^{3+} environment in crystalline solids can be obtained by combining the luminescence data obtained from recorded excitation spectra, emission spectra, and luminescence lifetimes, as discussed below. Selective excitation of the Eu^{3+} ion from the $^7F_0$ ground state to the $^5D_0$ excited state, which both are non-degenerate due to their J = 0 nature, allows for the determination of the number of non-equivalent species present in the solid matrix. In an excitation spectrum (integrated luminescence intensity as a function of excitation energy) of the $^7F_0 \rightarrow {}^5D_0$ transition, one singlet signal is obtained for every Eu^{3+} species present in the system. The signal position, gives a first indication of the local environment of the respective Eu^{3+} species, where a stronger ligand field generally results in a lower energy transition and consequently in a stronger bathochromic shift of the signal.[26,27]

For Eu^{3+} incorporation in the synthetic monazites only one singlet species corresponding to the structural incorporation of the dopant on the host lanthanide site is expected.

Selective excitation of the Eu^{3+} species in the solid matrix yields emission spectra and luminescence lifetimes of the single species. The emission spectrum allows for identification of the site symmetry in the host by making use of the splitting pattern of especially the $^5D_0 \rightarrow {}^7F_1$ and $^5D_0 \rightarrow {}^7F_2$ transitions. The crystal-field perturbation splits up the ^7F_J terms in a number of crystal field levels that depends on the symmetry class. For crystal fields of orthorhombic or lower symmetries, the 2J+1 degeneracy is completely lifted.[18] Thus, the monazite cation lattice site with a monoclinic (C_1) symmetry would result in a full 3-fold and 5-fold splitting of the $^7F_1$ and $^7F_2$ bands, respectively, for Eu^{3+} incorporation.

The Eu^{3+} luminescence lifetime, τ, has been correlated with the number of coordinating water molecules around the ion in solution through a linear empirical relationship, the so-called Horrocks equation[28,29], Equation 1.

$$n(H_2O)\ [\text{water molecules}] = 1.07\ [\text{water molecules} \cdot \text{ms}] \times \tau^{-1}\ [\text{ms}^{-1}] - 0.62 \qquad (1)$$

For an incorporated ion without hydration water molecules in the first coordination sphere and in the absence of other quench processes (e.g. metal-to-metal energy transfer) the expected luminescence lifetime according to Eq. 1 is ~1.7 ms. However, significantly longer lifetimes (> 3 ms) have been reported for incorporated Eu^{3+} species.[30-32]

In the present work time-resolved laser fluorescence spectroscopy (TRLFS) for the collection of Eu^{3+} excitation and emission spectra was performed with a pulsed Nd:YAG (Spectra Physics) pumped dye laser set-up (Radiant Dyes Narrow Scan K) by directly exciting the Eu^{3+} ion from the ground $^7F_0$ state to the emitting $^5D_0$ state. The emitted luminescence emission light was directed into a monochromator (Acton SpectraPro 300i) with a 300- or 1200 lines/mm grating and the emission was monitored with an intensified CCD camera (Princeton Instruments) 10 μs after the exciting laser pulse in a time window of 10 ms. The laser pulse

energy and the exact excitation wavelength were monitored in every measurement with optical power meter (Newport 1918-R) and wavelength meter (High Finesse WS-5), respectively. To achieve the desired spectral resolution the solid samples were cooled to approximately 10 K in a helium refrigerated cryostat. Luminescence lifetime measurements were performed at two temperatures (10 K and at room temperature, RT) by monitoring the luminescence emission as a function of delay time (up to 12 ms) between the laser pulse and the camera gating. Lifetime measurements at 10 K were conducted with the laser set-up described above. The room temperature TRLFS measurements were performed with a Nd:YAG pumped OPO laser system (Powerlite Precision II 9020 - PANTHER EX OPO, Continuum). Eu^{3+} was excited at 394 nm and the time-resolved emission signal was directed into a monochromator (Oriel MS 257) with a 300 lines/mm grating followed by detection with an intensified CCD camera (Andor iStar).

3 Results and discussion

3.1 Eu^{3+} incorporation in $LnPO_4$ monazites

Excitation spectra of $LaPO_4$, $SmPO_4$, and $GdPO_4$ monazites doped with 500 ppm Eu^{3+} are presented in Figure 2 together with the excitation spectrum of pure $EuPO_4$. $PrPO_4$ and $NdPO_4$ doped with Eu^{3+} did not yield any detectable europium luminescence signal due to strong metal-metal quenching induced by the host lanthanides. The Eu^{3+} luminescence quenching phenomenon observed in some of the investigated solids will be discussed separately in the following section.

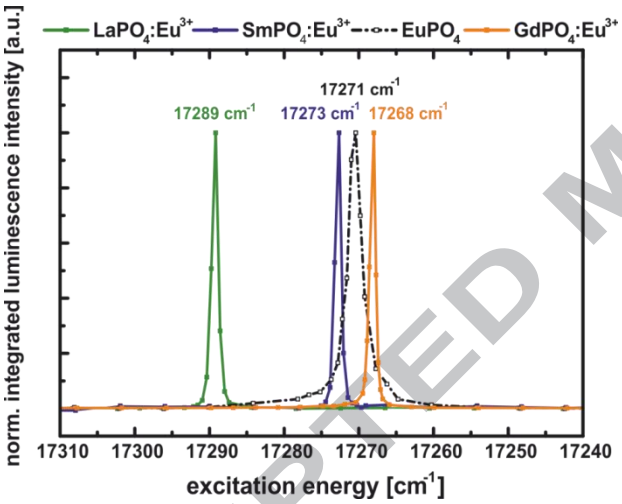

Figure 2: Eu^{3+} excitation spectra of the $^7F_0 \rightarrow {}^5D_0$ transition in $LaPO_4$, $SmPO_4$, and $GdPO_4$ monazites doped with 500 ppm Eu^{3+} (colored lines) and pure $EuPO_4$ (black line).

The Eu^{3+}-doped monazites show one narrow excitation peak with a half width of around 1 cm^{-1}, corresponding to Eu^{3+} incorporation on the host lattice sites in the crystalline monazite structure. The size of the host cation can be seen to influence the recorded Eu^{3+} luminescence signal in two ways: A slight excitation line narrowing can be seen across the monazite series (excluding $EuPO_4$) with a FWHM of 1.03 cm^{-1}, 0.95 cm^{-1}, 0.92 cm^{-1} for Eu^{3+}-doped $LaPO_4$, $SmPO_4$, and $GdPO_4$, respectively. This can be explained by slight local distortions of the monazite crystal lattice around the incorporated Eu^{3+} ion, which is more pronounced for larger differences between the host and dopant cation radii, see Table 1.

Table 1: Host lanthanide radii and average Ln···O bond distances in monazites.

Monazite	Ln^{3+}radius $r_{Ln(III)}^{IX}$ [Å]*	Average Ln···O distance [Å]**
$LaPO_4$	1.216	2.5787
$CePO_4$	1.196	2.5554
$PrPO_4$	1.179	2.5396
$NdPO_4$	1.163	2.5242
$PmPO_4$	1.144	2.5106†
$SmPO_4$	1.132	2.4988
$EuPO_4$	1.120	2.4878
$GdPO_4$	1.107	2.4760

*from Shannon[23]

**calculated from the refined monazite structures in Ni et al.[33]

†predicted value from spectroscopic data, this study.

Furthermore, as the Ln···O bond length decreases from $LaPO_4$ toward $GdPO_4$ (Table 1) the ligand field effect that the oxygen atoms exert on the incorporated Eu^{3+} ion increases, leading to a visible bathochromic shift of the excitation signal. This shift follows a linear trend as a function of both ionic radius of the host cation and Ln···O bond distance (Figure 3), with excellent accuracy (R^2 = 0.99999 and R^2 = 0.99984, respectively). The average bond distances are calculated from the nine Ln·· O distances in the LnO_9 polyhedron obtained from the refined monazite structures in Ni et al.[33].

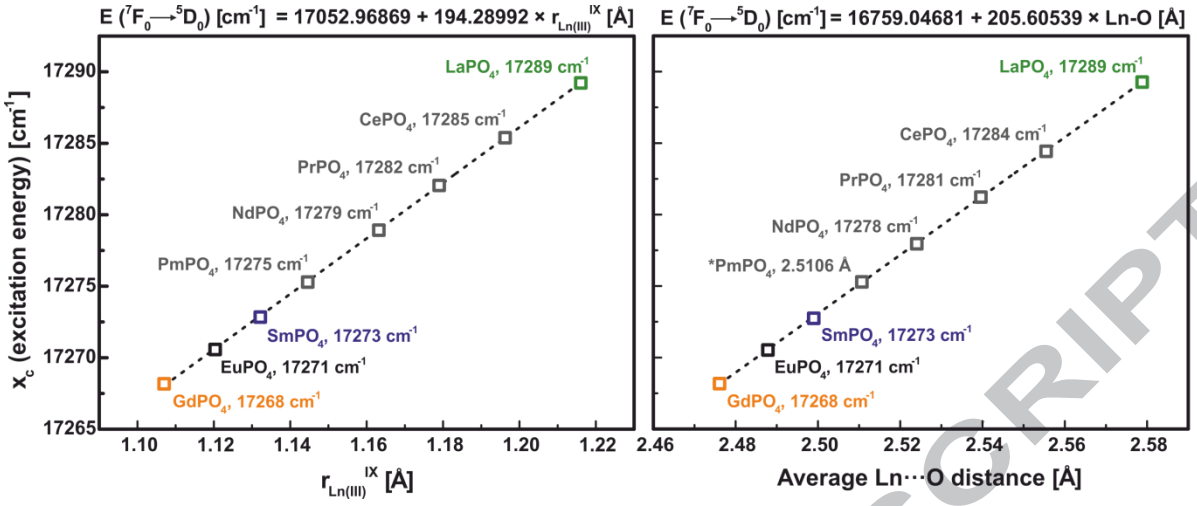

Figure 3: The Eu^{3+} excitation energy plotted as a function of the host cation radius (left) and average Ln···O distance in the monazite structure (right). Colored and black squares represent experimental data. Gray squares represent predicted values for the Eu^{3+} excitation energy or average Pm···O distance (*).

The linear fit of the experimental data (colored squares for Eu^{3+}-doped monazites, black square for pure $EuPO_4$ monazite) yield an expression for the excitation energy which can be calculated when either the lanthanide cation radius (Equation 2) or the average Ln·· O distance in the monazite (Equation 3) is known.

$$E(^7F_0 \rightarrow {}^5D_0)[cm^{-1}] = 17052.96869 + 194.28992 \cdot r_{Ln(III)^{IX}}[Å] \quad (2)$$

$$E(^7F_0 \rightarrow {}^5D_0)[cm^{-1}] = 16759.04681 + 205.60539 \cdot Ln \cdots O\,[Å] \quad (3)$$

Provided that the linear trend is valid throughout the monazite series these equations can be used to predict the excitation energies for Eu^{3+} incorporation in monazites for which no experimental data is available ($CePO_4$, $PrPO_4$, $NdPO_4$, $PmPO_4$). In addition, we can apply the results to predict the Pm·· O distance for $PmPO_4$, for which no crystallographic structure has been reported. The predicted excitation energy for Eu^{3+}- doped $PmPO_4$ can be calculated with the known ionic radius of Pm^{3+} using Equation 2. Subsequently, a Pm·· O bond distance of

2.5106 Å can be calculated using that excitation energy and Equation 3. The predicted values are indicated in Figure 3 in gray. For a summary of all determined and predicted excitation energies the reader is referred to the S.I. (Table S1).

When exciting europium at the excitation peak maximum in Figure 2, the emission spectra and luminescence lifetimes of the incorporated Eu^{3+} ion can be recorded, Figure 4.

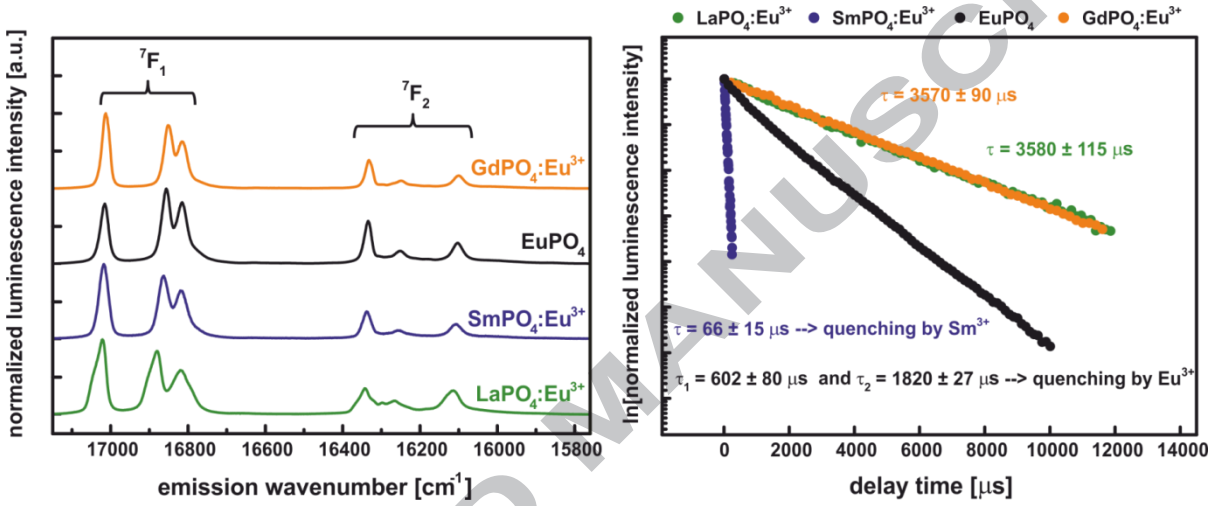

Figure 4: Eu^{3+} emission spectra (left) and luminescence lifetimes (right) in $LnPO_4$ monazites.

The emission spectra show a full 3-fold and 5-fold splitting of the $^7F_1$ and $^7F_2$ bands, respectively, corresponding to Eu^{3+} incorporation on a low symmetry site, in accordance with the monoclinic (C_1) lattice site in the monazites. The relative intensities of these bands reflect the coordination symmetry around the Eu^{3+} ion.[34,35] The $^5D_0 \rightarrow {}^7F_2$ transition has a predominant electric dipole character that is sensitive to changes in the ligand environment. In contrast, the $^5D_0 \rightarrow {}^7F_1$ transition retains its magnetic dipole character even in low symmetry systems and its intensity is not significantly influenced by the ligand environment.[36] Thus, when the site symmetry decreases, the relative intensity of the hypersensitive transition ($^5D_0 \rightarrow {}^7F_2$) increases, resulting in a larger $^7F_2/^7F_1$ ratio. For the Eu^{3+} doped monazites a decrease in the $^7F_2/^7F_1$ ratio can be seen when going from $LaPO_4$ toward $GdPO_4$ with a ratio of 0.50 for $LaPO_4$, 0.41 for $SmPO_4$, and 0.37 for $GdPO_4$. This behavior can be explained by

the slight distortion of the crystal lattice accommodating a dopant with a dissimilar cation radius and the subsequent lowering of the site symmetry, as already explained above in connection to the observed excitation line narrowing. The largest difference of approximately 8%, between the size of the host and dopant cation radii, is observed for Eu^{3+} incorporation in $LaPO_4$, while a difference of just above 1 % applies for Eu^{3+} incorporation in $SmPO_4$ and $GdPO_4$.

The luminescence lifetimes recorded at 10 K of Eu^{3+} incorporated in $LaPO_4$ and $GdPO_4$ decay monoexponentially with lifetimes of 3580 ± 115 µs and 3570 ± 90 µs, respectively. The long lifetimes speak for a full loss of the Eu^{3+} hydration sphere upon incorporation in the monazite lattice, as can be expected after sintering of the samples at 1450°C. The lifetime recorded for Eu^{3+} incorporation in $SmPO_4$ (66 ± 15 µs) and the lifetimes obtained for pure $EuPO_4$ (602 ± 80 µs and 1820 ± 27 µs) are significantly shorter than 3600 µs, pointing toward quenching of the luminescence signal by e.g. the lanthanide neighbor atoms. As we can exclude quenching by water molecules due to the thermal treatment of the lanthanide phosphates, Eu^{3+} luminescence must be quenched through a different mechanism. This quenching behavior will be discussed in detail in the following section.

3.2 Eu^{3+} luminescence quenching in $LnPO_4$ monazites

As discussed in the previous chapter, no Eu^{3+} luminescence could be detected in Eu^{3+}-doped $NdPO_4$ and $PrPO_4$ monazites, while significantly shortened lifetimes in $SmPO_4$ and $EuPO_4$ were recorded in comparison to the non-quenched Eu^{3+}-doped $LaPO_4$ and $GdPO_4$ hosts (Figure 4, right).

Various phenomena causing luminescence quenching of Eu^{3+} in a solid matrix have been reported, ranging from e.g. lattice defects in the solid structure[37] to excitation energy transfer to impurity ions present in the solid phase or metal-metal energy transfer between the dopant

and host cations[38]. In the present study, the monazite synthesis was carried out under controlled conditions where the chemicals, synthesis steps, sintering conditions and sample handling have been kept constant. Thus, lattice defects and the presence of impurity ions should be very comparable within the monazite end-member series, which would imply that other quench mechanisms such as metal-metal energy transfer between Eu^{3+} and the lanthanide host cations are responsible for the observed differences in the luminescence properties of Eu^{3+}. Metal-metal energy transfer can take place either via radiative energy transfer or through interionic processes involving direct excitation energy transfer between the two lanthanide ions without absorption or emission of photons.[39] Radiative energy transfer is only possible when one of the europium emission transitions $^5D_0 \rightarrow {}^7F_J$ overlap with the absorption transition of another lanthanide, and in this case it is only the emission of the overlapping transition that is affected. The non-radiative relaxation process can be divided into resonant and non-resonant excitation energy transfer induced by either multipolar or exchange interactions between the interacting ions.[39] Resonant multipolar energy transfer occurs when the amount of energy delivered by the Eu^{3+} dopant is reasonably close to the amount of energy accepted by the host lanthanide. In the non-resonant case a fraction of excitation energy is either exchanged with the phonon field of the host lattice or transferred to a third ion. The extent of quenching through multipolar energy transfer has been shown to decrease exponentially with increasing energy mismatch, i.e. a larger band gap between donor and acceptor states.[40,41] The band gap in the present case is defined as the energy difference between the Eu^{3+} $^5D_0 \rightarrow {}^7F_J$ emission transitions and the closest matching absorption transition of the accepting lanthanide. An exponential correlation cannot be deduced from our luminescence data but it is evident that the quenching of the Eu^{3+} luminescence is dependent on the size of the band gap ΔE, according to:

$$\Delta E(Eu^{3+} \rightarrow Nd^{3+}) \sim \Delta E(Eu^{3+} \rightarrow Pr^{3+}) < \Delta E(Eu^{3+} \rightarrow Sm^{3+}) < \Delta E(Eu^{3+} \rightarrow Eu^{3+})$$

The corresponding transitions are indicated in Figure 5, using identically colored arrows to indicate the $^5D_0$ to $^7F_6$ (purple), $^7F_5$ (orange), and $^7F_0$ (green) emission transitions and the closest matching absorption transitions. The arrow length is adapted to the individual band gaps, i.e. the length of the arrow indicating an emission transition does not necessarily match the arrow length of the closest matching absorption transition. For the corresponding transition energies the reader is referred to the S.I., Table S2. For Eu^{3+}, the absorption transition is assumed to be $^7F_0 \rightarrow {}^7F_6$, which plays an important role in e.g. the quenching of Tm^{3+} luminescence[42,43]. It is however, clear that for every europium $^5D_0 \rightarrow {}^7F_J$ emission transition a perfectly matched $^7F_J \rightarrow {}^5D_0$ absorption transition is available and the energy band gap is, thus, zero. Energy transfer between matching transitions, however, does not lead to the observed quenching of the Eu^{3+} luminescence.

La^{3+} is omitted from the figure due to the absence of *f* electrons and consequently *f-f* transitions. In addition, electronic transitions in La^{3+} from 5*p* to 4*f* or 5*d* states require substantially higher energies to occur and they will, thus, not interfere with the electronic transitions under consideration in the present study.

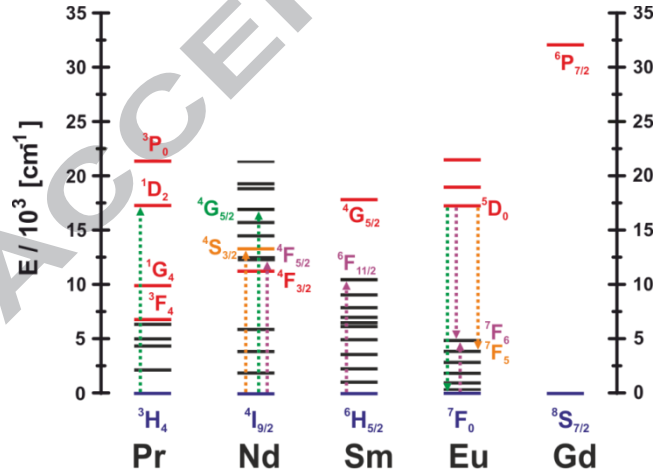

Figure 5: Partial energy level diagram of the lanthanides investigated in the present study. Emitting states are denoted in red. The colored arrows denote potential non-radiative transitions between donor and acceptor atoms, respectively. The figure is adapted from Bünzli and Piguet[44].

In both $NdPO_4$ (transitions indicated with purple and orange arrows) and $PrPO_4$ (green arrow) the energy gap difference is small, i.e. approximately 10 cm^{-1} in $NdPO_4$ and 60 cm^{-1} in $PrPO_4$. In neither of these solids any detectable luminescence from Eu^{3+} was observed. In $SmPO_4$ the band gap is approximately 1900 cm^{-1} and in $EuPO_4$ 7400 cm^{-1}. In these solids Eu^{3+} luminescence was visible but luminescence lifetimes were reduced. The effect is significantly stronger in $SmPO_4$ (τ = 66 ± 15 µs) than in $EuPO_4$ (τ_1 = 602 ± 80µs, τ_2 = 1820 ± 27 µs). In $LaPO_4$ and $GdPO_4$ non-radiative quenching is unlikely due to the absence of accepting energy levels below and close to the emitting $^5D_0$ term and the decay constants determined in these systems can be treated as entirely radiative deexcitation. In $NdPO_4$ and $PrPO_4$ where the energy band gap is very small, it is reasonable to assume that Eu^{3+} luminescence could be completely quenched by resonant multipolar energy transfer. In $SmPO_4$ and $EuPO_4$ non-resonant excitation energy transfer induced by either multipolar or exchange interactions should be considered due to the larger differences between the emission and absorption transitions. For the Sm^{3+} - Eu^{3+} couple, several studies reporting phonon assisted multipolar energy transfer between the lanthanide cations can be found[45-47]. Thus, it is reasonable to assume that the same energy transfer mechanism applies to Eu^{3+}-doped $SmPO_4$ monazite.

For multipole interactions the rate of energy transfer, k_{ET}, between a donor and acceptor atom can be correlated with their interatomic distance R_{DA}, according to equation 4:[48]

$$k_{ET} = k_D \left[\frac{R_0}{R_{DA}}\right]^S = \frac{1}{\tau_D}\left[\frac{R_0}{R_{DA}}\right]^S \quad (4)$$

Here, s = 6, 8, and 10, respectively, for dd, dq, and qq interactions. R_0 is the critical distance (also known as the Förster radius for dd-interactions in (bio)organic systems)[49], i.e. the distance at which the rate of energy transfer equals the reciprocal value of the lifetime of the donor level in the absence of acceptor ions, τ_D. In case of dipole-dipole interactions that usually feature large interaction lengths of several tens of angstroms[50,51], a critical distance R_0 can be calculated when both the quenched (τ_{DA}) and unquenched lifetimes are known:

$$R_0{}^6 = R_{DA}{}^6(\frac{\tau_D}{\tau_{DA}} - 1) \quad (5)$$

Using the unquenched lifetime of 3570 µs found for Eu^{3+} incorporation in $GdPO_4$, the average interatomic distance of 4.13 Å between two adjacent samarium atoms (connected to one another through an oxygen atom of a phosphate anion), and the quenched lifetime of 66 µs for Eu^{3+}-doped $SmPO_4$ the critical distance R_0 is found to be 8.02 Å. This distance is similar to reported critical distances for Eu^{3+} incorporation in solid matrices such as $KGdTiO_4$ (R_0 = 8.46 Å)[52] or Y_2O_3 (R_0=8.4 Å)[53].

In order to assess the self-quenching mechanism in $EuPO_4$, a critical distance should be calculated. Equation 6[54,55] provides a simple way of obtaining an estimate for the critical distance R_0 below which no concentration quenching of Eu^{3+} occurs.

$$R_0 \approx 2 \times \left(\frac{3V}{4\pi x_c N}\right)^{1/3} \quad (6)$$

Here N is the number of Eu^{3+} cations in the $EuPO_4$ unit cell (N = 4), V is the volume of the unit cell (2.902×10^{-28} m^3 derived from the $EuPO_4$ unit cell parameters reported in Ni et al.[33]), and x_c is the critical concentration ($Ln_{1-x}Eu_xPO_4$) beyond which concentration quenching is observed. As the focus of this paper has not been on resolving the quench mechanisms occurring in the Eu^{3+} doped monazites, we have not conducted a Eu^{3+} concentration dependent series for one of the monazites where a critical concentration could have been extracted. However, preliminary luminescence data on a $La_{1-x}Eu_xPO_4$ solid solution series indicates a slight deviation from the unquenched lifetime obtained for Eu^{3+} doped $LaPO_4$ for an x value of 0.1[56]. Thus, by assuming a x_c value of 0.1 (also often encountered for Eu^{3+} in various solid matrices[53,57-58]) a critical distance of 11.2 Å is obtained. This value is much larger than expected for the exchange interaction[18,59], indicating that electric multipolar interactions would be responsible for the observed self-quenching in $EuPO_4$. For a definite

assessment of the quench mechanism, however, a series of $Ln_{1-x}Eu_xPO_4$ solids should be synthesized for the extraction of a more accurate critical concentration.

Finally, in $EuPO_4$ the non-resonant energy transfer must be accompanied by a significant involvement of the phonon field or third party (impurity) ions to account for the excess excitation energy that is not dissipated through the acceptor absorption transition ($^7F_0 \rightarrow {}^7F_6$). To get an idea of the significance of lattice vibrations in the monazite solids and their impact on the luminescence lifetimes, room temperature lifetime measurements were conducted and compared to the lifetimes obtained at 10 K, Figure 6. In $SmPO_4$ no Eu^{3+} signal was obtained at RT, thus, a comparison cannot be made.

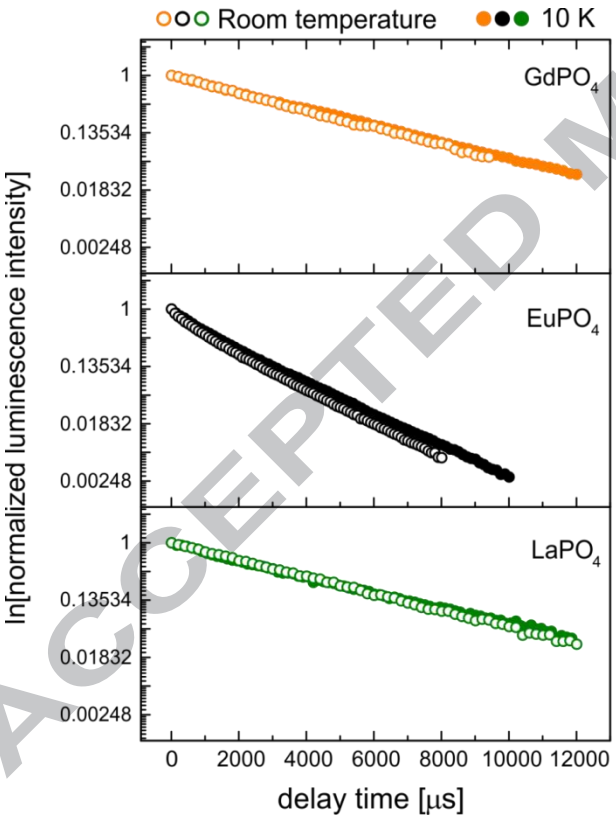

Figure 6: Comparison of lifetimes collected at room temperature (open symbols) and at 10 K (solid symbols) for $LaPO_4$, $EuPO_4$, and $GdPO_4$.

The difference between RT and 10 K lifetimes is in general very small. The absolute reduction of the lifetime in these solids lies between 130 µs and 285 µs, leading to a relative difference of 5-8 % in $LaPO_4$, $GdPO_4$, and for the longer component in $EuPO_4$. The largest

relative difference is observed for the shorter lifetime in $EuPO_4$ which is reduced from 602±80µs at 10 K to 465±60 µs at RT, i.e. a decrease of around 20%. Due to the overall low influence of temperature on the lifetimes, however, phonon assisted energy transfer dissipating an excess energy equivalent to 7400 cm^{-1} is not very likely. Thus, for $EuPO_4$ impurities are expected to play a role in the deexcitation process. For Eu^{3+}-doped $SmPO_4$ with a lifetime of 66µs at 10 K a similar absolute decrease of the lifetime as observed for the other monazite solids would be enough to completely quench the Eu^{3+} luminescence signal. It is not likely that the phonon field in $SmPO_4$ would behave very differently to the other monazites, however, for a definite assessment of the phonon contribution to the quenching of the Eu^{3+} luminescence signal and the subsequent contribution of third party ions, Eu^{3+} luminescence lifetimes in the $SmPO_4$ solid should be recorded at additional temperatures between RT and 10 K.

4 Conclusions

The systematic decrease of the Ln^{3+} host cation radius and Ln···O bond distance in the series of synthesized Eu^{3+}-doped monazites ($LaPO_4$-$GdPO_4$) has enabled the study of Eu^{3+} luminescence properties related to size differences between host and dopant cation radii and the ligand field effect, in this case exerted by the oxygen ligands, in the monazite solids. We have shown that the slight distortion of the monazite crystal lattice around the Eu^{3+} dopant, when going from very similar host- and dopant cation radii (such as Eu^{3+} doped in $GdPO_4$) towards larger differences (Eu^{3+} doped in $LaPO_4$) causes a slight broadening of the Eu^{3+} excitation peak and an increase of the $^7F_2/^7F_1$ emission peak ratio. Furthermore, the increasing influence of the oxygen ligand field on the Eu^{3+} dopant as the Ln···O bond distance decreases across the monazite series, results in a systematic shift of the Eu^{3+} excitation peak position. This trend shows a linear dependence of both the Ln^{3+} host cation radius and the Ln···O bond distance. This dependence was used to predict the energy band gap of the $^7F_0 \rightarrow {}^5D_0$ transition for those Eu^{3+}-doped monazites that were not synthesized in the present study ($CePO_4$ and $PmPO_4$) or the monazites that did not show any Eu^{3+} luminescence due to strong metal to metal induced quenching ($NdPO_4$ and $PrPO_4$). In addition, we could apply the predicted excitation peak position for Eu^{3+}-doped $PmPO_4$ to further predict the average Pm·· O distance in $PmPO_4$, for which no crystallographic structure has been reported. To our knowledge, a perfect linear relationship between the dopant to ligand distance and the energy band gap has not been observed previously for Eu^{3+} incorporation in solid materials with different host cations. If a linear trend can be found to apply for other solid materials, the possibility for energy band gap predictions based on the known host to oxygen ligand distance could open new possibilities in the construction and tailoring of luminescent materials for various applications. For such predictions, however, the presence and proximity of other luminescent centers around the dopant ion must be accounted for as shown in the present study. Due to the absence of structural or chemical differences in the series of investigated monazites, we can

attribute the degree of Eu^{3+} luminescence quenching by neighboring lanthanide cations to the size of the energy band gap between the donor atom emission transition and the acceptor atom absorption transition alone. However, it has to be noted that the quenching behavior in the present study applies to a doping of 500 ppm (0.05%) Eu^{3+} in the synthetic monazite solids. A different degree of quenching is likely to be obtained when increasing the dopant concentration in the monazites. Finally, the observed phenomena and the lack of Eu^{3+} luminescence in certain monazites do not influence the performance of the solid phases as suitable hosts for the trivalent dopant. A perfect substitution of the Eu^{3+} dopant for the host cation sites in all investigated monazites was obtained, independent of the size of the host cation, promoting the use of these ceramic phases as hosts phases, for example for the immobilization of trivalent dopants, such as the minor actinides Am^{3+} and Cm^{3+}.

Acknowledgements

The authors would like to thank Jacqueline Holthausen for the synthesis of the monazites. Dr. Gerhard Geipel is thanked for his assistance related to the laser set-up. This work was supported by the German Federal Ministry of Education and Research (BMBF) [grant number 02NUK021] and the Helmholtz Gemeinschaft Deutscher Forschungszentren by supporting the Helmholtz-Nachwuchsgruppe "Structures and Reactivity at the Water/Mineral Interface" [grant number VH-NG-942].

Supporting Information: Details on the reagents used for the monazite synthesis are given. XRD spectra of all synthesized monazite end-members are presented in Figure S1. The experimental and predicted excitation energies as well as the predicted Pm···O distance are compiled in Table S1. Table S2 summarizes the transition energies of the Eu^{3+} $^5D_0 \rightarrow {}^7F_J$ emission transitions and various absorption transitions of the host lanthanides.

5 References

1 P. Yang, Z. Quan, C. Li, Z. Hou, W. Wang and J. Lin, *J. Solid State Chem.*, 2009, **182**, 1045–1054.

2 M. Guan, J. Sun, M. Han, Z. Xu, F. Tao, G. Yin, X. Wei, J. Zhu and X. Jiang, *Nanotechnology*, 2007, **18**,415602.

3 S. Rodriguez-Liviano, A. I. Becerro, D. Alcántara, V. Grazú, J. M. de la Fuente and M. Ocaña, *Inorg. Chem.*, 2013, **52**, 647−654.

4 L. Zhang, G. Jia, H. You, K. Liu, M. Yang, Y. Song, Y. Zheng, Y. Huang, N. Guo and H. Zhang, *Inorg. Chem.*, 2010, **49**, 3305–3309.

5 I. W. Donald, B. L. Metcalfe and R. N. J. Taylor, *J. Mater. Sci.*, 1997, **32**, 5851–5887.

6 R. C. Ewing and L. Wang, *Rev. Mineral. Geochem.*, 2002, **48**, 673–699.

7 G. Deissmann, S. Neumeier, G. Modolo and D. Bosbach, *Mineral. Mag.*, 2012, **76**, 2911–2918.

8 N. Dacheux, N. Clavier and R. Podor, *Am. Mineral.*, 2013, **98**, 833–847.

9 F. Brandt, S. Neumeier, T. Schuppik, Y. Arinicheva, A. Bukaemskiy, G. Modolo and D. Bosbach, *Prog. Nucl. Energy*, 2014, **72**, 140–143.

10 Y. Arinicheva, A. Bukaemskiy, S. Neumeier, G. Modolo and D. Bosbach, *Prog. Nucl. Energy*, 2014, **72**, 144–148.

11 C. M. Gramaccioli and T. V. Segalstad, *Am. Mineral.*, 1978, **63**, 757–761.

12 D. Bregiroux, R. Belin, P. Valenza, F. Audubert and D. Bernache-Assollant, *J. Nucl. Mater.*, 2007, **366**, 52–57.

13 K. S. Holliday, C. Babelot, C. Walther, S. Neumeier, D. Bosbach and T. Stumpf, *Radiochim. Acta*, 2012, **100**, 189–195.

14 O. Terra, N. Dacheux, F. Audubert and R. Podor, *J. Nucl. Mater.*, 2006, **352**, 224–232.

15 D. Bregiroux, O. Terra, F. Audubert, N. Dacheux, V. Serin, R. Podor and D. Bernache-Assollant, *Inorg. Chem.*, 2007, **46**, 10372–10382.

16 R. P. Rao and D. J. Devine, *J. Lumin.*, 2000, **87–89**, 1260–1263.

17 F. Du, R. Zhu, Y. Huang, Y. Tao and H. J. Seo, *Dalton Trans.*, 2011, **40**, 11433–11440.

18 K. Binnemans, *Coord. Chem. Rev.*, 2015, **295**, 1–45.

19 L. G. Van Uitert, *J. Electrochem. Soc.*, 1960, **107**, 803–806.

20 A. Rapaport, V. David, M. Bass, C. Deka and L. A. Boatner, *J. Lumin.*, 1999, **85**, 155–161.

21 L. Li and S. Zhang, *J. Phys. Chem. B*, 2006, **110**, 21438–21443.

22 C. C. Santos, I. Guedes, C.-K. Loong, L. A. Boatner, A. L. Moura, M. T. de Araujo, C. Jacinto and M. V. D. Vermelho, *J. Phys. D: Appl. Phys.*, 2010, **43**, 025102.

23 R. D. Shannon, *Acta Cryst.*, 1976, **A32**, 751–767.

24 T. Roncal-Herrero, J. D. Rodríguez-Blanco, E. H. Oelkers and L. G. Benning, *J. Nanopart. Res.*, 2011, **13**, 4049–4062.

25 K. Binnemans and C. Görller-Walrand, *J. Rare Earths*, 1996, **14**, 173–180.

26 M. Albin and W. D. Horrocks, *Inorg. Chem.*, 1985, **24**, 895–900.

27 G. R. Choppin and Z. M. Wang, *Inorg. Chem.*, 1997, **36**, 249–252.

28 W. D. Horrocks and D. R. Sudnick, *J. Am. Chem. Soc.*, 1979, **101**, 334–340.

29 T. Kimura, G. R. Choppin, Y. Kato and Z. Yoshida, *Radiochim. Acta*, 1996, **72**, 61–64.

30 M. Marques Fernandes, M. Schmidt, T. Stumpf, C. Walther, D. Bosbach, R. Klenze and T. Fanghänel, *J. Colloid Interface Sci.*, 2008, **321**, 323–331.

31 M. Schmidt, T. Stumpf, M. Marques Fernandes, C. Walther and T. Fanghänel, *Angew. Chem. Int. Ed.*, 2008, **47**, 5846–5850.

32 M. Schmidt, T. Stumpf, C. Walther, H. Geckeis and T. Fanghänel, *Dalton Trans.*, 2009, **33**, 6645–6650.

33 Y. Ni, J. M. Hughes and A. N. Mariano, *Am. Mineral.*, 1995, **80**, 21–26.

34 R. Reisfeld, E. Zigansky and M. Gaft, *Mol. Phys.*, 2004, **102**, 1319–1330.

35 Z. Zhao, Q. G. Zeng, Z. M. Zhang and Z. J. Ding, *J. Lumin.*, 2007, **122-123**, 862–865.

36 F. S. Richardson, *Chem. Rev.*, 1982, **82**, 541–552.

37 T. Aitasalo, P. Dereń, J. Hölsä, H. Jungner, J.-C. Krupa, M. Lastusaari, J. Legendziewicz, J. Niittykoski and W. Stręk, *J. Solid State Chem.*, 2003, **171**, 114–122.

38 L. G. Van Uitert and L. F. Johnson, *J. Chem. Phys.*, 1966, **44**, 3514–3522.

39 A. Richter, *Laser parameters and performance of Pr^{3+}-doped fluorides operating in the visible spectral region*, Cuvillier Verlag, Göttingen, 2008.

40 N. Yamada, S. Shionoya and T. Kushida, *J. Phys. Soc. Jpn.*, 1972, **32**, 1577–1586.

41 T. Miyakawa and D. L. Dexter, *Phys. Rev. B*, 1970, **1**, 2961–2969.

42 J. T. Vega-Durán, L. A. Díaz-Torres, M. A. Meneses-Nava, J. L. Maldonado-Rivera and O. Barbosa-García, *J. Phys. D: Appl. Phys.*, 2001, **34**, 3203–3208.

43 R. Lisiecki, W. Ryba-Romanowski and T. Łukasiewicz, *Appl. Phys. B*, 2006, *83*, 255–259.

44 J.-C. G. Bünzli and C. Piguet, *Chem. Soc. Rev.*, 2005, **34**, 1048–1077.

45 D. Kouyate, J. C. Ronfard-Haret and J. Kossanyi, *J. Lumin.*, 1993, **55**, 209–216.

46 Y.-C. Fang, S.-Y. Chu, P.-C. Kao, Y.-M. Chuang and Z.-L. Zeng, *J. Electrochem. Soc.*, 2011, **158**, J1–J5.

47 H.-Y. Lin and S.-Y. Chu, *ECS J. Solid State Sci. Technol.*, 2013, **2**, R121–R125.

48 M. Inokuti and F. Hirayama, *J. Chem. Phys.*, 1965, **43**, 1978–1989.

49 T. Förster, *Ann. Physik*, 1948, **2**, 55–75.

50 N. Felorzabihi, P. Froimowicz, J. C. Haley, G. Rezanejad Bardajee, B. Li, E. Bovero, F. C. J. M. van Veggel and M. A. Winnik, *J. Phys. Chem. B*, 2009, **113**, 2262–2272.

51 M. Lunz, A. L. Bradley, V. A. Gerard, S. J. Byrne, Y. K. Gun'ko, V. Lesnyak and N. Gaponik, *Phys. Rev. B*, 2011, **83**, 115423.

52 N. Zhang, C. Guo, J. Zheng, X. Su and J. Zhao, *J. Mater. Chem. C*, 2014, **2**, 3988–3994.

53 M. K. Chong, K. Pita and C. H. Kam, *J. Phys. Chem. Solids*, 2005, **66**, 213–217.

54 G. Blasse, *Phys. Lett. A*, 1968, **28**, 444–445.

55 G. Blasse, *Philips Res. Repts.*, 1969, **24**, 131–144.

56 own unpublished data†

57 X. Zhang and H.-J. Seo, *J. Alloys Compd.*, 2010, **503**, L14–L17.

58 A. Yousif, S. Som, V. Kumar and H. C. Swart, *Mater. Chem. Phys.*, 2015, **166**, 167–175.

59 D. L. Dexter, *J. Chem. Phys.*, 1953, **21**, 836–850.

†data provided to reviewers

Graphical abstract

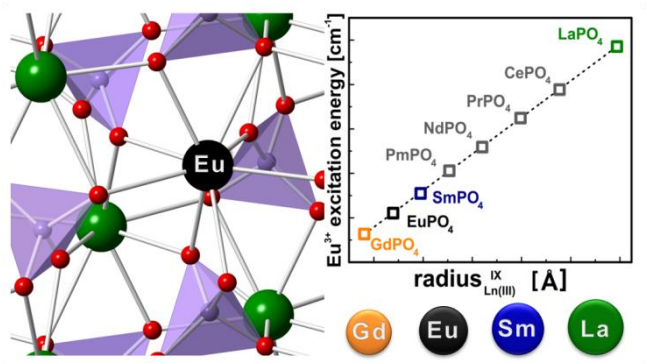

Supporting Information

Using Eu^{3+} as an atomic probe to investigate the local environment in $LaPO_4$-$GdPO_4$ monazite end-members

Nina Huittinen[1], Yulia Arinicheva[2], Moritz Schmidt[1], Stefan Neumeier[2], Thorsten Stumpf[1]

[1]Helmholtz-Zentrum Dresden - Rossendorf, Institute of Resource Ecology, Bautzner Landstraße 400, 01328 Dresden, Germany

[2]Forschungszentrum Jülich GmbH, Institute of Energy and Climate Research, Nuclear Waste Management and Reactor Safety (IEK-6), 52425 Jülich, Germany

As starting materials for the monazite synthesis the following reagents were used: $La(NO_3)_3 \cdot 6H_2O$ (Alfa Aesar), $Pr(NO_3)_3 \cdot 6H_2O$ (Aldrich), $Nd(NO_3)_3 \cdot 6H_2O$ (Aldrich), $Sm(NO_3)_3 \cdot 6H_2O$ (Alfa Aesar), $Eu(NO_3)_3 \cdot 6H_2O$ (Alfa Aesar), $Gd(NO_3)_3 \cdot 6H_2O$ (Aldrich) and analytical grade 85% H_3PO_4 (Merck).

The crystallinity and phase purity of the synthesized products were characterized by XRD. All measured XRD spectra are compiled in Figure S1.

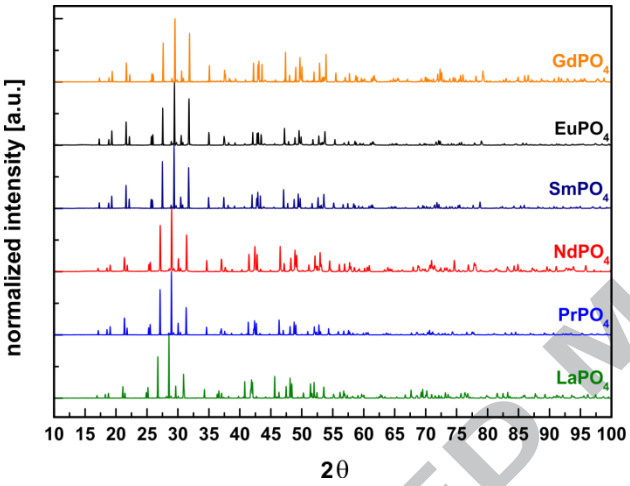

Figure S1: XRD spectra of all synthesized monazite end-members

From the linear equations obtained by plotting the Eu^{3+} excitation peak position as a function of host cation radius or average Ln·· O distance, the excitation energies for Eu^{3+} incorporation in monazites for which no experimental data could be obtained ($CePO_4$, $PrPO_4$, $NdPO_4$, $PmPO_4$) have been calculated. In addition, the excitation peak position for Eu^{3+}-doped $PmPO_4$ could be further used to predict the average Pm·· O distance in $PmPO_4$, for which no crystallographic structure has been reported. The experimentally derived and predicted values for the excitation energies and the Pm·· O distance are tabulated in Table S1 below.

Table S1: Experimentally derived and predicted values for the Eu^{3+} excitation energies and the Pm·· O distance in the synthetic monazite end-members.

Monazite	Experimental data Eu^{3+} excitation energy [cm^{-1}]	Predicted data* Equation 2 / Equation 3
$LaPO_4$	17289	-
$CePO_4$	-	17285 / 17284
$PrPO_4$	-	17282 / 17281
$NdPO_4$	-	17279 / 17278
$PmPO_4$	-	E = 17275 / R = 2.5106
$SmPO_4$	17273	-
$EuPO_4$	17271	-
$GdPO_4$	17268	-

*Eu^{3+} excitation energies are given in cm^{-1} and Pm···O distance in Å.

The band gap, i.e. the energy difference between the Eu^{3+} $^5D_0 \rightarrow {}^7F_J$ emission transitions and the closest matching absorption transition of the accepting lanthanide has been calculated from available data in Martin et al. 1978. For the sake of consistency, the calculations have been done with the published emission transition energy of 17270 cm^{-1} for the $^5D_0 \rightarrow {}^7F_0$ transition of the Eu^{3+} ion despite the experimentally derived values for this transition ranging from 17268 to 17289 cm^{-1} in the various Eu^{3+}-doped monazites in the present study. The transition energies and energy gap differences are compiled in Table S2.

Table S2: Transition energies for the Eu^{3+} $^5D_0 \rightarrow {}^7F_J$ emission transitions, chosen monazite host lanthanide absorption transitions and the energy difference (ΔE) of the emission- and absorption transitions.

Emission transition Eu^{3+}	Transition energy [cm^{-1}]*	
$^5D_0 \rightarrow {}^7F_6$	12330	
$^5D_0 \rightarrow {}^7F_5$	13360	
$^5D_0 \rightarrow {}^7F_0$	17270	
Absorption transition Pr^{3+}	Transition energy [cm^{-1}]*****	ΔE (emission–absorption) [cm^{-1}]
$^3H_4 \rightarrow {}^1D_2$	17334	$^5D_0 \rightarrow {}^7F_0$ (17270) – 17334 = –64
Absorption transition Nd^{3+}	Transition energy [cm^{-1}]*****	ΔE (emission–absorption) [cm^{-1}]
$^4I_{9/2} \rightarrow {}^4F_{5/2}$	12320	$^5D_0 \rightarrow {}^7F_6$ (12330) – 12320 = 10
$^4I_{9/2} \rightarrow {}^4S_{3/2}$	13370	$^5D_0 \rightarrow {}^7F_5$ (13360) – 13370 = –10
$^4I_{9/2} \rightarrow {}^4G_{5/2}$	16980	$^5D_0 \rightarrow {}^7F_0$ (17270) – 16980 = 290

Absorption transition Sm^{3+}	Transition energy [cm^{-1}]*	ΔE (emission–absorption) [cm^{-1}]
$^6H_{5/2} \rightarrow {}^6F_{11/2}$	10470	$^5D_0 \rightarrow {}^7F_6$ (12330) – 10470 = 1860
Absorption transition Eu^{3+}	Transition energy [cm^{-1}]*	ΔE (emission–absorption) [cm^{-1}]
$^7F_0 \rightarrow {}^7F_6$	4940	$^5D_0 \rightarrow {}^7F_6$ (12330) – 4940 = 7390

*The transition energies are taken from Martin, W. C., Zalubas, R., and Hagan, L. 1978 Atomic Energy Levels – The Rare-Earth Elements: The Spectra of Lanthanum, Cerium, Praseodymium, Neodymium, Promethium, Samarium, Europium, Gadolinium, Terbium, Dysprosium, Holmium, Erbium, Thulium, Ytterbium, and Lutetium. Institute for Basic Standards, National Bureau of Standards, Washington D.C. 20234.